

Microstructure and mechanical properties of in situ TiB₂/7055 composites synthesized by direct magnetochemistry melt reaction

Long-hua ZHONG, Yu-tao ZHAO, Song-li ZHANG, Gang CHEN, Shuai CHEN, Yong-hong LIU

School of Materials Science and Engineering, Jiangsu University, Zhenjiang 212013, China

Received 2 July 2012; accepted 13 November 2012

Abstract: In situ TiB₂/7055 composites were successfully synthesized via magnetic chemical direct melt reaction from 7055 (Al–3B)–Ti system. The phase composition and the microstructure of the composites were investigated by XRD, OM and SEM technologies, and the mechanical and wear properties were tested. The results indicate that with the pulsed magnetic field assistance, the morphologies of in situ TiB₂ particles are mainly hexagonal-shape or nearly spherical, the sizes are less than 1 μm, and the distribution of the matrix is uniform. Compared the microstructures of the 7055 aluminum matrix composites synthesized without pulsed magnetic field, the average size of α(Al) phase with pulsed magnetic field assistance is decreased from 20 to 10 μm, the array of the second phase is changed from continuous net-shape to discontinuous shape. With the pulsed magnetic field, the tensile strengths of the composites are enhanced from 310 to 330 MPa, and the elongations are increased from 7.5% to 8.0%. In addition, compared with matrix alloy, the wear mass loss of the composites is decreased from 111 to 78 mg under a load of 100 N for 120 min.

Key words: in situ composite; magnetic chemistry; microstructure; mechanical properties

1 Introduction

Nowadays, with the increasing concern about energy saving and demands of applying advanced structures in aerospace, military, automobile and electronic area, particle-reinforcement aluminum matrix composites (PRAMCs) are more and more attractive for the material scientists, because of their low density, high specific stiffness, strong wear resistance, reduced thermal expansion coefficient and high thermal conductivity [1–4]. Among all the fabrication techniques of PRAMCs, casting process is widely used due to its excellent near-net-shape production capability, economical viability and versatility. Near-net-shape casting process can be classified as ex situ (where the reinforcing particles are added into the melt as powders) or in situ ones (where particles are synthesized within the melt). Compared with the traditional ex situ composites, the in situ reinforced aluminum matrix composites possess more advantages in both microstructures and mechanical properties, such as clean interfaces, strong interfacial

bonding, fine particles and uniform distribution in matrix [5–8].

In recent years, TiB₂ as reinforcement for aluminum matrix composites has been extensively investigated due to its high stiffness, hardness and thermodynamic stability in contrast to most ceramics. The addition of TiB₂ to a metal matrix can greatly improve stiffness, hardness, and wear resistance without apparent loss of thermal expansion coefficient and conductivities compared with other ceramic reinforcements. There are several approaches to synthesize in situ TiB₂/Al composites. Among them, stir casting is the most economical viability. Researchers have done a massive research effort in synthesizing the TiB₂ particle-reinforcement aluminum matrix composites, and fine TiB₂/Al composites have been successfully fabricated by different measures [9–14]. But most of the previous reports were focused on fluoride salt and oxide as resources of Ti and B. For instance, LE et al [15] developed TiB₂/A356 composites successfully via the melt in situ reaction, where the exothermic reaction occurred when two kinds of reactants (K₂TiF₆ and KBF₄)

Foundation item: Projects (50971066, 51174098) supported by the National Natural Science Foundation of China; Project (2008-46) supported by Jiangsu Provincial “333” Project of Training the High-level Talents Foundation, China; Project (BE2009127) supported by Jiangsu Provincial Science Supporting Item, China; Project (2011-11) supported by Jiangsu Provincial College Excellent Science and Technology Innovation Team, China; Project (kjsmxc0903) supported by Jiangsu Key Laboratory of Tribology Project, China; Project (1201220072) supported by Jiangsu Province Undergraduate Practice-Innovation Training, China

Corresponding author: Yu-tao ZHAO; Tel: +86-511-8791919; E-mail: zhaoyt@ujs.edu.cn

DOI: 10.1016/S1003-6326(13)62761-2

were added into the aluminum melt. LU et al [16] fabricated in situ TiB_2 reinforced Al alloy composites from Al–4% Cu matrix, TiO_2 and B_2O_3 powders [16]. However, very few researchers have used master alloys as reactant materials.

The use of master alloys as reactants exhibits several advantages over commonly used powders and salts. The reaction process is simple and materials are fully utilized, while in salt method the reactants are not fully utilized due to the formation of slag at high temperatures, and complicated reaction process leads to formation of other unwanted byproducts. The fabrication of in situ composites via powders as reactants is at high temperature conditions. However, the master alloys as reactants can be completed at relatively low temperature conditions and the yield ratio is high [17,18], but the direct melt reaction using master alloys requires long stirring time at high temperatures in order to obtain the full incorporation and thorough reaction of the added reactants. Thus, the magnetic field as one of the fabrication techniques is used for synthesizing the $\text{TiB}_2/7055$ composites, because the strong vibration effects of magnetic field can accelerate the reaction process, refine grains, decrease segregation and lead to fine and more uniform particle distribution [19].

In the present work, the $\text{TiB}_2/7055$ composites are fabricated from Al–3B master alloy and Ti powder via melt in situ reaction with the pulsed magnetic field assistance. The distribution and morphology of in situ reinforcements, the microstructures and mechanical properties of the composites are investigated. The effects of pulsed magnetic field on the microstructures and properties of the composites are analyzed, and the mechanisms are discussed.

2 Experimental

The raw materials were titanium powder (purity 75%, average size 100 μm), Al–3B and commercial 7055 master alloy. The nominal compositions of experimental 7055 and Al–3B master alloy are listed in Table 1.

Table 1 Compositions of 7055 and Al–3B master alloy (mass fraction, %)

Alloy	Zn	Mg	Cu	Zr	Fe	Mn	Si	Al
7055	8.0	2.2	2.2	0.2	≤ 0.10	≤ 0.05	≤ 0.15	Bal.
Alloy	B		Fe	Others		Al		
Al–3B	2.94		0.32	0.10		Bal.		

The 7055 matrix alloy was melted in a graphite crucible ($d70 \text{ mm} \times 85 \text{ mm} \times 160 \text{ mm}$) heated by an

electrical resistance furnace, and certain amount of Al–3B master alloy was added into the molten alloy at 973 K. When the temperature of the melt was 1113 K, Ti powder was added (mole ration of Ti to B is 1:2.1) and incorporated by mechanical stirring. During the in situ reaction, the impulse magnetic field system (WY1600) was turned on and the frequency was fixed at 25 Hz and the magnetic current intensity was 150 A. After holding the reaction temperature at 1123 K for 30 min, the melt was degassed by hexachloroethane degasifying agent, and then poured into a mould with 14 mm in inside diameter and 80 mm in length. After being cooled to the room temperature in air, the specimens were cut for XRD and SEM analysis, as well as mechanical properties test. The sizes of the specimens for tensile and wear are shown in Fig. 1 and Fig. 2, respectively.

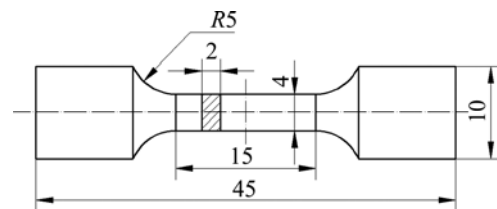


Fig. 1 Sizes of tensile specimen (unit: mm)

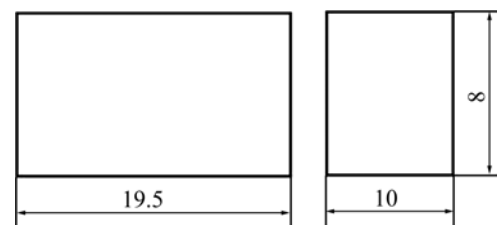


Fig. 2 Sizes of wear specimen (unit: mm)

The X-ray diffraction (XRD, Rigaku D/max2500) was used to determine the phase component. Optical microscope (OM, LEICA DFC420) and scanning electron microscope (SEM, JEOL-JSM-7001F) were employed to observe the morphologies of reinforcement phases and tensile fracture surfaces. The tensile properties tests were carried out at room temperature by a computer-controlled electronic tensile testing machine (DWD–200) at a strain rate of $1.67 \times 10^{-4} \text{ s}^{-1}$ according to the ASTM E8 standard. Wear tests were conducted under a load of 100 N with sliding velocity of 0.42 m/s by a wear apparatus (MG–2000) at room temperature.

3 Results and discussion

3.1 XRD and microstructure analyses

Figure 3 shows the XRD pattern of in situ $\text{TiB}_2/7055$ composites synthesized from 7055

(Al–3B)–Ti system with pulsed magnetic field assistance. As shown in Fig. 3, the in situ composites are composed of $\alpha(\text{Al})$, TiB_2 , CuAl_2 and MgZn_2 phases, which indicate the existence of in situ TiB_2 particulates. Due to no obvious diffraction peaks of AlB_2 and Al_3Ti in Fig. 3, the reaction occurring in the 7055 (Al–3B)–Ti system is complete.

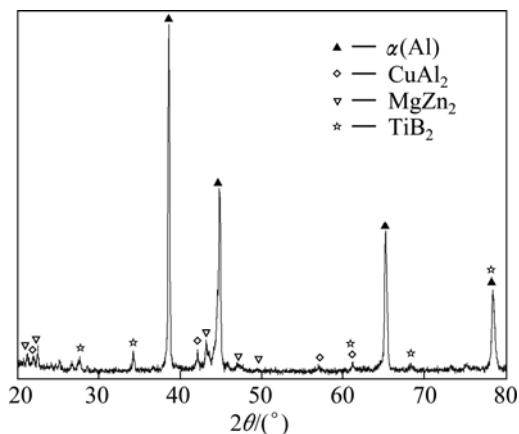


Fig. 3 XRD pattern of $\text{TiB}_2/7055$ composites

According to the above XRD pattern and Refs. [17] and [18], the possible reaction taken place in the 7055 (Al–3B)+Ti system can be illustrated as follows:



The in situ reaction starts from the initiation of cracks and voids on the external surfaces of Al_3Ti with diffusion of free B atoms into these sites, and the number of sites for the reaction is increased with dissolution of Al_3Ti particles, so that the rate of the reaction is raised with forming finer TiB_2 particles. Further, the possibility of reaction between Al_3Ti and AlB_2 cannot be ignored, because of the instability of Al_3Ti and AlB_2 at high temperatures.

In this research, considering the grain refinement of Al–3B master alloy and the mass loss at high temperatures, excess boron (mole ration of Ti to B is 1:2.1) was added into the melt to ensure the full response of Al_3Ti [20]. As shown in Eqs. (2) and (3), excess boron also promotes the formation of TiB_2 and inhibits the existence of Al_3Ti , but the temperature of Al–3B master alloy is usually 973–1033 K, which will lead to the mass loss of boron at high temperatures. When the reaction is complete, there is barely a trace of boron in the composites, so the AlB_2 phase is not obviously found in the results. These are correspondence with the XRD pattern and the microstructures.

Figure 4 shows the morphologies and distributions of the TiB_2 particles in 7055 matrix composites. As shown in Fig. 4(a), the morphology of the particles is typically hexagonal or nearly spherical and the size is less than 1 μm , and there are clear interfaces between the TiB_2 particles and 7055 matrix. Figures 4(b) and (c) show the distributions of TiB_2 particles fabricated with different additions. It can be seen that the particles fabricated with 3% TiB_2 are smaller and distribute uniformly than that with 5% TiB_2 , and the morphologies of the particles are typically spherical. When the mass fraction of TiB_2 particles is 5%, the particles agglomerate to form some particle clusters, and the size of some particles even reaches 1 μm .

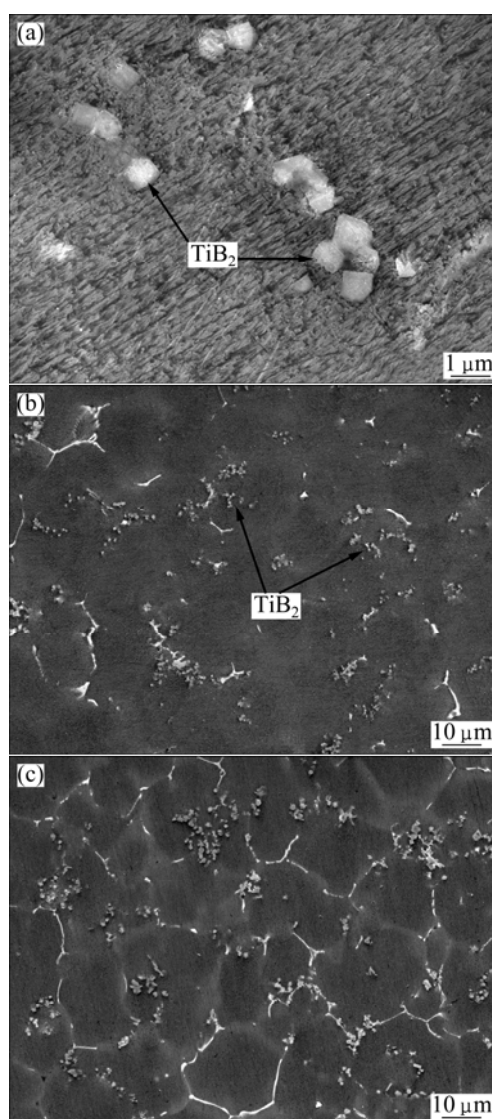


Fig. 4 SEM images of as-prepared composites: (a) Morphology of particles; (b) With 3% TiB_2 addition; (c) With 5% TiB_2 addition

3.2 Influence of pulsed magnetic field

Figure 5 shows the SEM images of the in situ $\text{TiB}_2/7055$ composites with 3% TiB_2 synthesized without

or with pulsed magnetic field assistance. With the pulsed magnetic field, a clear beneficial effect, in terms of the more uniform distribution of particles in the matrix, and a reduction in particle size to a sub-micron level are obtained. In addition, the grain size is significantly refined and the agglomeration of particles in matrix is reduced by the applied magnetic field. These are due to the strong vibration effects from the magnetic field, which are helpful to prevent existing clusters from clustering and breaking up. Furthermore, the larger electromagnetic force also gives rise to considerable agitation of the melt which improves significance of the diffusion between reactants leading to fine and more uniform particles [21].

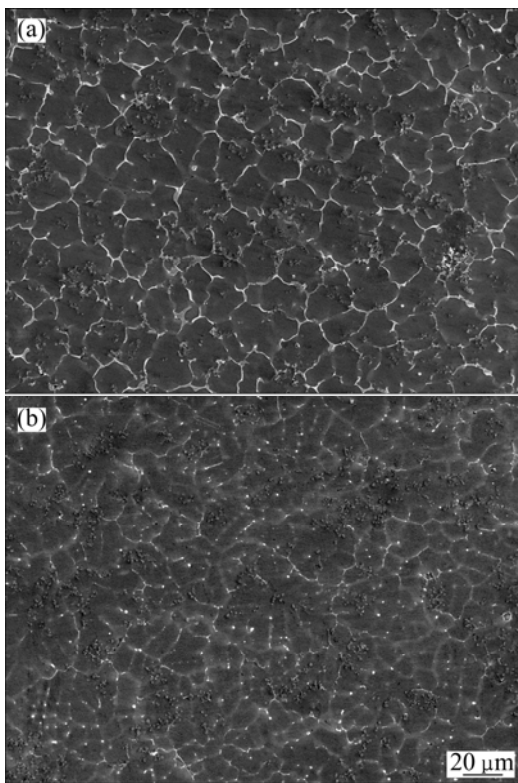


Fig. 5 SEM images of TiB₂/7055 composites synthesized without pulsed magnetic field assistance (a) and with pulsed magnetic field assistance (b)

Based on the solidification theories [22], the nucleation near the mold and the liquid surface is an important source of nucleus. When the pulsed magnetic field is applied, the forced convection leads to the liquid surface to increase, so more nuclei are formed near the mold and the liquid surface. The broken dendrite crystal, which is caused by magnetic field, is another important source of nucleus. The movement velocity of nuclei and low temperature melt is accelerated by the forced convection, so that the solute field and temperature field become more uniform. Thus, the whole melt is quickly

cooled and the tendency of remelting of nuclei is reduced. Overall, with the assistance of pulsed magnetic field, the grain size is significantly refined and the TiB₂ particles become finer and more uniform, as shown in Fig. 5(b).

3.3 Tensile properties

The tensile properties of the cast matrix and in situ TiB₂/7055 composites synthesized without or with pulsed magnetic field assistance tested under a load of 5 kN at tensile velocity of 1 mm/min are listed in Table 2. The results indicate that the tensile strength of the composites is significantly enhanced from 285 to 310 MPa. When the pulsed magnetic field is applied, the tensile strength of the cast composites is increased from 310 MPa to 333 MPa. The improvement in tensile strength of the composites can be imputed to the interaction between TiB₂ particles and dislocations; these reinforcement particles act as barriers to the movement of dislocations under the load, leading to higher tensile strength of the composites. Compared with matrix alloy, the ductility of the in situ composites synthesized with pulsed magnetic field shows no obvious decrease, which can be attributed to the grain refinement and coordination mechanism for micro-mechanics, and can retard the crack propagation during tensile deformation. Grain refinement may cause a great number of grains in a specific volume, and the deformation distributed uniformly with the grains, which lead to the better plasticity.

Table 2 Tensile properties of cast matrix and composites

Material	Magnetic field	Tensile strength/MPa	Elongation/%
7055 alloy	Without	285	8.3
3%TiB ₂ /7055	Without	310	7.5
3%TiB ₂ /7055	With	333	8.0

3.4 Tensile fracture surface

Figure 6 shows the SEM images of tensile fracture surface of the cast matrix alloy and composites synthesized without or with pulsed magnetic field. As shown in Fig. 6(a), more dimples and tearing edges are observed, and few brittle areas are seen in 7055 cast matrix. This type of fracture is more consistent in materials with relatively high ductility. In Fig. 6(b), the number of observed dimples is decreased, and more brittle areas are observed on the composites fracture surface. As shown in Fig. 6(c), with the pulsed magnetic field, the number of dimples is increased and the size is smaller, which indicates that the ductility is retained. The variation of the tensile fracture surface is correspondence with the mechanical properties variations of the composites.

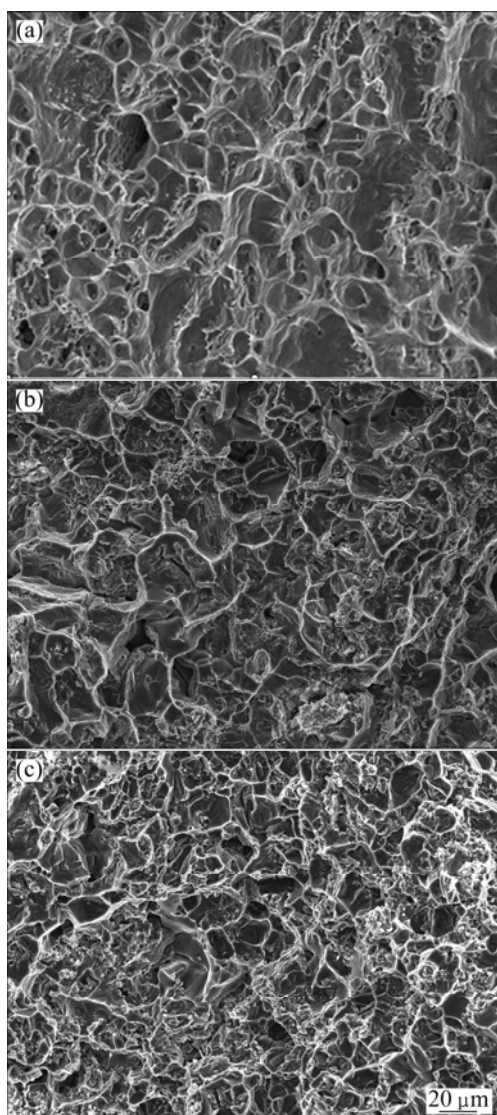


Fig. 6 SEM images of tensile fracture surface: (a) Cast matrix; (b) Composites synthesized without magnetic field; (c) Composites synthesized with magnetic field

3.5 Dry sliding properties of composites

In order to evaluate the wear resistance of the composites, the wear mass loss of the composites which were fabricated without or with pulsed magnetic field is tested under a load of 100 N and sliding velocity of 0.42 m/s at different sliding time. Figure 7 shows variations in wear mass loss of the composites and matrix alloy as a function of sliding time. As shown in Fig. 7, compared with matrix alloy, the wear mass loss of the composites decreases in a given sliding time, and increases nearly linearly with the sliding time. In particular, when the sliding time is 120 min, the wear mass loss of composites synthesized with pulsed magnetic field is 78 mg, while that of matrix alloy is 111 mg. This can be attributed to the high stiffness, hardness and thermodynamic stability of TiB_2 particles, and the addition of TiB_2 particles can greatly improve the wear resistance of matrix alloy.

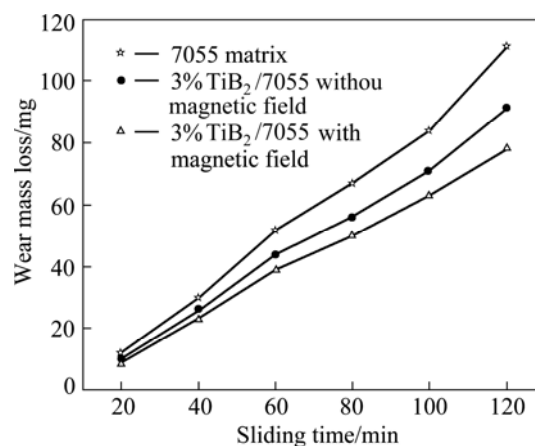


Fig. 7 Wear mass loss of composites and matrix alloy as function of sliding time

Figure 8 shows the SEM micrographs of the worn surface of the matrix alloy and composites under a load of 100 N, sliding velocity of 0.42 m/s and sliding time of 120 min.

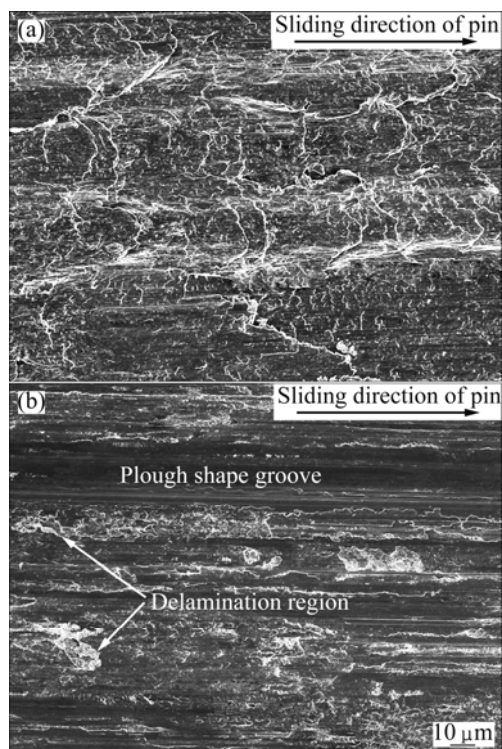


Fig. 8 SEM images of worn surface: (a) Matrix alloy; (b) Composites synthesized with magnetic field

As shown in Fig. 8(a), the distinct plastic-deformation layers and torn-up layers are observed. The wear action shows the adhesion wear character. With the addition of TiB_2 particles, the plastic-deformation layers and torn-up layers also exist (see Fig. 8(b)). In addition, the plough shape grooves along the sliding direction created by the cutting action of the abrasive grains and

some delamination of the tribo oxide layer regions are obviously observed. The wear actions show a hybrid wear mechanism: adhesion wear, abrasive grains wear and mild oxidative wear [23]. During the wear process, the friction would produce plastic deformation and friction heat. As TiB_2 is well known for its high stiffness, hardness and thermodynamic stability, the particles on the worn surface can hinder the plastic deformation, which will lead to the discoordination of strain rate and temperature between TiB_2 particles and 7055 matrix. As a result, the strain gradient and temperature gradient may cause dynamic changes of worn surface shown in Fig. 8.

4 Conclusions

1) The $\text{TiB}_2/7055$ composites are successfully fabricated from 7055 (Al–3B)–Ti system via magnetochemistry in situ melt reaction.

2) With the pulsed magnetic field, the morphologies of the in situ TiB_2 particles are mainly hexagonal-shape or nearly spherical, the size is less than 1 μm , and the distribution in the matrix is uniform. In addition, the grain size is significantly refined, the average size of $\alpha(\text{Al})$ phase is decreased from 20 to 10 μm , and the array of the second phases is changed from continuous net-shape to discontinuous shape.

3) The tensile strength of the composites with 3% TiB_2 is enhanced from 310 to 333 MPa with pulsed magnetic field, and the elongation is increased from 7.5% to 8.0%.

4) The addition of TiB_2 particles can greatly improve the wear resistance of matrix. In particular, under a load of 100 N, sliding velocity of 0.42 m/s and sliding time of 120 min, the wear mass loss of composites synthesized with pulsed magnetic field decreases from 111 to 78 mg.

References

- [1] TJONG S C, MA Z Y. Microstructural and mechanical characteristics of in situ metal matrix composites [J]. *Materials Science and Engineering R*, 2000, 29(4): 49–113.
- [2] REDDY B S B, RAJASEKHAR K, VENU M, DILIP J J S, DAS S, DAS K. Mechanical activation-assisted solid-state combustion synthesis of in situ aluminum matrix hybrid ($\text{Al}_3\text{Ni}/\text{Al}_2\text{O}_3$) nanocomposites [J]. *Journal of Alloys and Compounds*, 2008, 465: 97–105.
- [3] DINAHARANA I, MURUGAN N, SIVA P. Influence of in situ formed ZrB_2 particles on microstructure and mechanical properties of AA6061 metal matrix composites [J]. *Materials Science and Engineering A*, 2011, 528: 5733–5740.
- [4] MAZAHERY A, SHABANI M O. Characterization of cast A356 alloy reinforced with nano SiC composites [J]. *Transactions of Nonferrous Metals Society of China*, 2012, 22(2): 275–280.
- [5] ZHU He-guo, MIN Jing, LI Jian-liang, AI Ying-lu, GE Liang-qi, WANG Heng-zhi. In situ fabrication of ($\text{Al}_2\text{O}_3+\text{Al}_3\text{Zr}$)/Al composites in an Al–ZrO₂ system [J]. *Composites Science and Technology*, 2010, 70(15): 2183–2189.
- [6] ZHANG Yi-jie, MA Nai-heng, WANG Hao-wei, LE Yong-kang, LI Xian-feng. Damping capacity of in situ TiB_2 particulates reinforced aluminium composites with Ti addition [J]. *Materials and Design*, 2007, 28: 628–632.
- [7] ZHAO Yu-tao, ZHANG Song-li, CHEN Gang, CHENG Xiao-nong, DAI Qi-xun. ($\text{ZrB}_2+\text{Al}_2\text{O}_3+\text{Al}_3\text{Zr}$)_p/Al–4Cu composite synthesized by magneto-chemical melt reaction [J]. *Materials Science and Engineering A*, 2008, 487: 1–6.
- [8] ZHANG Song-li, ZHAO Yu-tao, CHEN Gang, CHENG Xiao-nong. ($\text{Al}_2\text{O}_3+\text{Al}_3\text{Zr}$)/A356 nanocomposites fabricated by magneto-chemistry in situ reaction [J]. *Journal of Alloys and Compounds*, 2009, 475: 261–267.
- [9] TEE K L, LU L, LAI M O. Improvement in mechanical properties of in situ Al– TiB_2 composite by incorporation of carbon [J]. *Materials Science and Engineering A*, 2003, 339: 227–231.
- [10] HAN Yan-feng, LIU Xiang-fa, BIAN Xiu-fang. In situ particulate reinforced near eutectic Al–Si alloy composites [J]. *Composites: Part A*, 2002, 33: 439–444.
- [11] JONAS F, JARFORS A E W. On the precipitation of TiB_2 in aluminum melts from the reaction with KBF_4 and K_2TiF_6 [J]. *Materials Science and Engineering A*, 2005, 413–414: 527–532.
- [12] XUE Jing, WANG Jun, SUN Bao-de. Research development of TiB_2 particle reinforced Al matrix composites [J]. *Material and Heat Treatment*, 2009, 38(24): 43–47. (in Chinese)
- [13] EMAMY M, MAHTA M, RASIZADEH J. Formation of TiB_2 particles during dissolution of TiAl_3 in Al– TiB_2 metal matrix composite using an in situ technique [J]. *Composites Science and Technology*, 2006, 66: 1063–1066.
- [14] AHMAD C, ALI K, NACI S. Production of in situ aluminum–titanium diboride master alloy formed by slag–metal reaction [J]. *Journal of Alloys and Compounds*, 2011, 509: 237–240.
- [15] LE Yong-kang, ZHANG Yi-jie, CHEN Dong. Microstructure and mechanical properties of in situ A356/ TiB_2 composites [J]. *Rare Metal Materials and Engineering*, 2006, 35(10): 1635–1638. (in Chinese)
- [16] LU L, LAI M O, SU Y, TEO H L. In situ TiB_2 reinforced Al alloy composites [J]. *Scripta Materialia*, 2001, 45: 1017–1023.
- [17] RAMESH C S, PRAMOD S, KESHAVAMURTHY R. A study on microstructure and mechanical properties of Al 6061– TiB_2 in-situ composites [J]. *Materials Science and Engineering A*, 2011, 528: 4125–4132.
- [18] RAMESH C S, AHAMED A, CHANNABASAPPA B H, KESHAVAMURTHY R. Development of Al 6063– TiB_2 in situ composites [J]. *Materials and Design*, 2010, 31: 2230–2236.
- [19] ZUO Yu-bo, CUI Jian-zhong, DONG Jie, YU Fu-xiao. Effects of low frequency electromagnetic field on the as-cast microstructures and mechanical properties of superhigh strength aluminum alloy [J]. *Materials Science and Engineering A*, 2005, 408: 176–181.
- [20] BIROL Y. Al–Ti–B grain refiners via powder metallurgy processing of Al/ $\text{K}_2\text{TiF}_6/\text{KBF}_4$ powder blends [J]. *Journal of Alloys and Compounds*, 2009, 480: 311–314.
- [21] MOLODOV D A, KONIJNENBERG P J. Grain boundary and grain structure control through application of a high magnetic field [J]. *Scripta Materialia*, 2006, 54: 977–981.
- [22] LIU Quan-kun. Basic principles of material forming [M]. Beijing: China Machine Press, 2004: 37. (in Chinese)
- [23] WANG Shu-qi, WEI Ming-xian, ZHAO Yu-tao. Effects of the tribo-oxide and matrix on dry sliding wear characteristics and mechanisms of a cast steel [J]. *Wear*, 2010, 269: 424–434.

磁化学熔体反应法合成 TiB₂/7055 复合材料的组织和性能

钟龙华, 赵玉涛, 张松利, 陈刚, 陈帅, 刘永红

江苏大学 材料科学与工程学院, 镇江 212013

摘要: 通过磁化学熔体反应法在 7055 (Al-3%B)-Ti 反应体系中成功制备 TiB₂/7055 复合材料。利用 XRD、OM 和 SEM 等分析检测技术研究复合材料的相组成和微观组织。结果表明, 脉冲磁场作用下生成的 TiB₂ 颗粒呈多边形或近球形, 尺寸小于 1 μm, 均匀分布于基体中。与未施加脉冲磁场的复合材料相比, 施加磁场后 α(Al)晶粒平均尺寸从 20 μm 减小到约 10 μm, 第二相从连续的网格状分布变为非连续性分布。在磁场作用下, 复合材料的抗拉强度从 310 MPa 提高到 333 MPa, 伸长率从 7.5%提高到 8.0%。此外, 与基体相比, 在载荷为 100 N, 磨损时间为 120 min 时, 复合材料的磨损量从 111 mg 降低到 78 mg。

关键词: 原位复合材料; 磁化学; 微观组织; 力学性能

(Edited by Xiang-qun LI)